Stacked Intelligent Metasurface Enhanced Integrated Communication and Computation

Qiyu Chen, Qiao Qi, *Member, IEEE*, Jiancheng An, *Senior Member, IEEE*, Zhaohui Yang, *Member, IEEE*, Xiaoming Chen, *Senior Member, IEEE*, Chongwen Huang, *Senior Member, IEEE*, and Chau Yuen, *Fellow, IEEE*

***Abstract*—As the sixth-generation (6G) networks evolve toward a deep integration of communication and computation (ICC), they face challenges of inherent interference and resource competition between heterogeneous services. To address this issue, this article investigates an uplink ICC system enhanced by a stacked intelligent metasurface (SIM), where SIM's unique multilayer structure transforms the wireless channel into a controllable, task-oriented medium. The system is designed to support the coexistence of over-the-air computation (AirComp) tasks, which require high-precision results, and traditional tasks that demand high-quality communication. To this end, we formulate a joint optimization framework aiming to minimize the total mean squared error (mse) of all computation tasks while strictly guaranteeing the communication quality of service (QoS). To solve the highly nonconvex problem of synergistically designing the system resources, we propose an efficient alternating optimization (AO) algorithm. Simulation results demonstrate that the proposed algorithm not only converges rapidly but also achieves up to a 95.2% reduction in total computation mse compared to an ICC system without SIM, while also significantly outperforming other benchmark schemes, validating the great potential of SIM in proactively managing multiservice conflicts and enabling efficient ICC.**

***Index Terms*—Integrated communication and computation, interference management, multiservice conflicts, sixth-generation (6G), stacked intelligent metasurface (SIM).**

I. Introduction

THE evolution toward sixth-generation (6G) wireless networks is driven by the need to support a burgeoning ecosystem of distributed intelligent applications, which requires moving beyond the traditional role of networks as simple data conduits [1]. Emerging paradigms such as federated learning (FL), real-time rendering for the metaverse, and collaborative decision-making in autonomous vehicle networks demand not only massive connectivity but also ultralow latency computation and ultrahigh reliability communication [2], [3]. Meeting these demands necessitates a fundamental paradigm shift, mandating a deep integration of communication and computation (ICC) in 6G wireless networks.

In this context, the conventional transmit and then compute approach, where vast amounts of raw data are first transmitted over limited radio resources to a central node for subsequent processing, has become one of the key bottlenecks that restricts the development of the wireless networks [4]. In particular, such sequential method introduces excessive latency and suffers from low spectral efficiency, rendering it unsuitable for the real-time demands of future intelligent services [5]. To address this issue, a prominent technique called over-the-air computation (AirComp) has emerged to achieve low-latency and high-accuracy computation in future wireless networks [6]. AirComp ingeniously leverages the waveform superposition property inherent in the multiple-access channel to directly compute functions of distributed data during uplink transmission [7]. By enabling concurrent transmission from multiple devices, the wireless channel itself becomes a shared analog computer, where the received signal at the base station (BS) naturally represents an aggregated result, such as the sum or average of sensor readings [8]. This computing-over-the-air paradigm not only offers a highly efficient one-shot solution for latency-critical tasks, such as large-scale data fusion and gradient aggregation in FL [9], [10], but also fundamentally transforms the communication process into a powerful computational resource, thereby significantly enhancing the spectral efficiency of the wireless network [11].

Despite the promising prospects of AirComp, the practical implementation of the ICC in 6G wireless networks faces a fundamental challenge that heterogeneous services with different requirements need to coexist within the same resource-constrained environment [12], [13]. On one hand, the successful execution of AirComp is highly contingent on signal precision, demanding the constructive alignment of multiple waveforms for accurate aggregation, and any other interference directly translates into computation error [14]. On the other hand, conventional communication tasks demand signal isolation, requiring strict quality of service

Received 24 October 2025; revised 14 December 2025; accepted 25 December 2025. Date of publication 29 December 2025; date of current version 26 March 2026. This work was supported in part by Zhejiang Provincial Natural Science Foundation of China under Grant LQN25F010014; in part by the Natural Science Foundation of China under Grant 62501222, Grant U21A20443, Grant 62231009, Grant 62331023, and Grant 62394292; in part by China National Key Research and Development Program under Grant 2025ZD1301900 and Grant 2021YFA1000500; in part by the Fundamental Research Funds for the Central Universities and Zhejiang University Global Partnership Fund; and in part by Ministry of Education, Singapore, under MOE Tier 2 under Grant T2EP50124-0032. *(Corresponding author: Qiao Qi.)*

Qiyu Chen and Qiao Qi are with the College of Information Sciences and Technology, Hangzhou Normal University, Hangzhou 311121, China (e-mail: cqqqy12138@163.com; qiqiao@hznu.edu.cn).

Jiancheng An and Chau Yuen are with the School of Electrical and Electronic Engineering, Nanyang Technological University, Singapore 639798 (e-mail: jiancheng_an@163.com; chau.yuen@ntu.edu.sg).

Zhaohui Yang, Xiaoming Chen, and Chongwen Huang are with the College of Information Science and Electronic Engineering, Zhejiang University, Hangzhou 310027, China, and also with Zhejiang Provincial Key Laboratory of Multi-Modal Communication Networks and Intelligent Information Processing, Hangzhou 310027, China (e-mail: yang_zhaohui@zju.edu.cn; chen_xiaoming@zju.edu.cn; chongwenhuang@zju.edu.cn).

Digital Object Identifier 10.1109/JIOT.2025.3649324

(QoS) guarantees to ensure reliable data decoding [15]. The concurrent operation of these services, one pursuing signal aggregation and the other signal separation, inevitably leads to intense mutual interference and resource competition [16].

To address this complex interference landscape, reconfigurable intelligent surfaces (RIS) have arisen as a powerful paradigm for proactively reshaping the wireless propagation environment [17]. In conventional communication-centric systems, a single-layer RIS, composed of numerous passive reflecting elements, has demonstrated considerable success in various applications [18]. By intelligently manipulating the phase of incident waves, it can enhance the signal quality for a target user, create spatial nulls to mitigate co-channel interference, or even enable secure transmissions by directing signals away from eavesdroppers [19], [20], [21]. However, the efficacy of a conventional RIS is constrained by several inherent limitations, which become particularly pronounced in the sophisticated multi-service scenarios of 6G wireless networks. First, its performance is often hampered by the double-fading effect, where the signal suffers significant path loss on both the transmitter-RIS and RIS-receiver links [22]. Second and significantly, its operation is akin to a single and smart mirror, which possesses limited degrees of freedom (DoFs) for wave manipulation [23]. This fundamentally restricts its ability to perform the nuanced, multiobjective channel shaping required by ICC. Specifically, a single-layer RIS may lack the capability to simultaneously create a highly correlated channel for the high-precision data aggregation of AirComp tasks while also generating an interference-free channel for the high-reliability data transmission of communication tasks [24]. The conflicting channel requirements, one demanding constructive signal alignment, and the other demanding destructive interference, often exceed the signal manipulation capacity of a single reflection [25]. Therefore, while beneficial for simpler interference scenarios, the conventional RIS architecture falls short of providing a robust solution for the deep-seated conflict in ICC systems.

Building on this architecture, the stacked intelligent metasurface (SIM) has recently been recognized as a more powerful paradigm for achieving sophisticated electromagnetic wave control [26]. Unlike a conventional single-layer RIS, a SIM is composed of several metasurface layers arranged in sequence, forming a 3-D structure capable of performing complex signal processing tasks in the electromagnetic domain [27]. Through successive modulation of the transmitted waves, the SIM can realize various functions such as spatial filtering, signal focusing, and multiple beam formation. This structure provides a much larger number of controllable parameters, which enables more precise manipulation of electromagnetic propagation [28]. Particularly, the high-dimensional solution space offered by the SIM is essential for resolving the core conflict in ICC systems. Although employing a static phase configuration within a coherence block, the massive DoFs inherent in the multi-layer architecture allow the SIM to accommodate disparate channel requirements simultaneously. By performing sophisticated wave-domain processing, the SIM can distinguish users based on their propagation paths, effectively constructing a task-oriented medium that constructively aligns signals for AirComp while concurrently establishing spatially isolated channels for communication, thus balancing computational accuracy and communication reliability.

A. Related Works and Motivation

The concept of the SIM has recently gained significant attention as a promising evolution from conventional single-layer RIS, offering substantially enhanced capabilities for wave manipulation in wireless communication systems. Initial pioneering works have primarily focused on leveraging SIM to improve the performance of various communication-centric systems. For instance, the authors in [29] investigated a SIM-assisted multi-user multiple-input single-output (MISO) system, demonstrating that the additional DoFs from the multi-layer architecture significantly enlarge the achievable rate region. Following this line, other studies have explored maximizing energy efficiency by jointly designing transmit power and phase shifts [30], and enhancing physical layer security by utilizing SIM's precise beamforming to create dedicated null spaces [31]. This trend is also expanding to other emerging 6G communication paradigms. For example, in non-terrestrial networks (NTNs), the work in [32] proposed deploying SIMs on low-Earth orbit satellites for wave-domain beamforming to reduce processing load. Similarly, authors in [33] investigated SIMs as holographic multiple-input multiple-output (MIMO)-aided access points to enhance uplink spectral efficiency in cell-free massive MIMO systems. Even in novel modalities like semantic communications, SIMs are modeled as electromagnetic neural networks (EMNNs) to perform the semantic inference using propagation waves as computing carriers [34].

While the aforementioned works demonstrate SIM's utility primarily in homogeneous tasks, they have largely overlooked the more complex challenge of managing heterogeneous multiservice coexistence in 6G wireless networks. Indeed, recent research has begun to leverage SIM to manage this multiservice integration, with notable progress in emerging paradigms such as integrated sensing and communication (ISAC). For instance, Niu et al. [35] investigated the application of SIM for ISAC systems, demonstrating its potential to jointly manage heterogeneous beams. Complementarily, the work in [36] focused on the practical resource allocation challenges within such frameworks, proposing a joint optimization of power allocation and discrete phase shifts for SIM-aided ISAC systems.

However, despite this progress in ISAC, the deep integration of ICC, particularly in the challenging uplink, remains substantially unexplored. This specific scenario exacerbates the inherent computation-communication conflict, where AirComp's need for constructive signal aggregation directly collides with the demand for strict signal isolation to protect communication QoS. Therefore, this article is motivated to bridge this gap. We noticed that the enhanced DoFs offered by the SIM's multi-layer architecture can transform the wireless channel from a source of conflict into a controllable, task-oriented medium. This unique capability is essential for the challenging uplink ICC scenario, as it allows for the management of conflicting heterogeneous service requirements. Thus, we aim to develop a holistic framework that leverages this capability to strike a

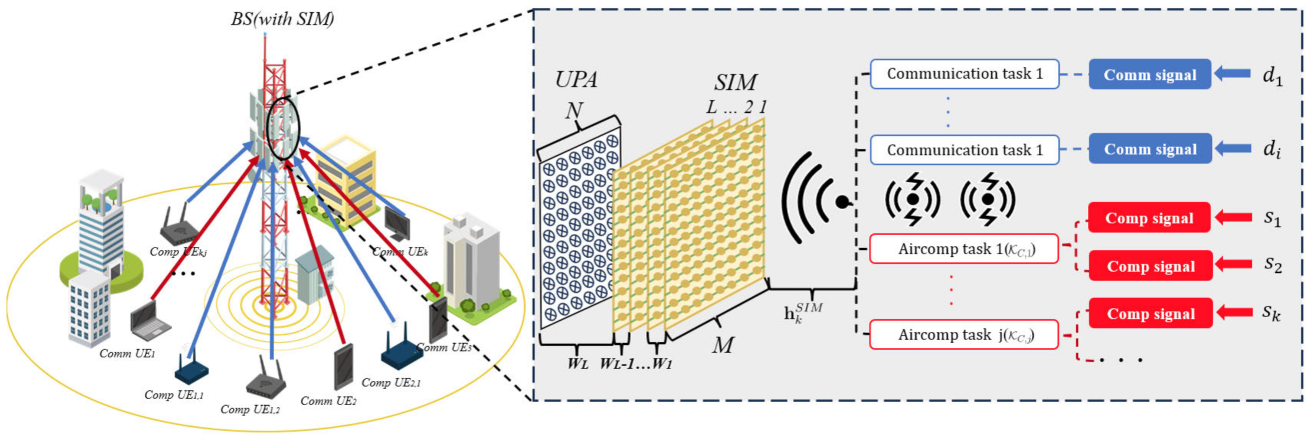

Fig. 1. Framework of SIM-enhanced uplink ICC.

balance between computational accuracy and communication reliability, thereby enhancing overall ICC system performance.

B. Contributions

In this article, we propose a novel framework for a SIM-enhanced uplink ICC system, designed to reconcile the conflicting requirements of high-precision AirComp and high-quality communication over the limited radio resource. The main contributions of this article are threefold as follows.

1) We propose a SIM-enhanced uplink ICC framework to resolve the inherent conflict between heterogeneous services. This framework leverages the SIM's unique multilayer structure to proactively reconfigure the propagation environment, which allows for the simultaneous creation of highly correlated channels beneficial for AirComp tasks and interference-free channels required for communication tasks.
2) We formulate a joint optimization problem to achieve the performance tradeoff between computation and communication under the same resource block. The problem aims to minimize the total computation mean squared error (mse) for all AirComp tasks while guaranteeing the QoS requirements for all communication tasks.
3) We develop an efficient iterative algorithm based on the alternating optimization (AO) framework to solve the formulated nonconvex optimization problem. The proposed algorithm tackles the challenge of highly coupled optimization variables by decomposing the original problem into three tractable subproblems, namely BS receiver design, transmit power allocation, and SIM phase shift optimization, which are then solved iteratively to find a high-quality solution.

C. Organization and Notations

The rest of this article is outlined as follows. Section II describes the system model for the SIM-enhanced uplink ICC network, detailing the end-to-end channel propagation and signal model. Section III formulates the joint optimization problem to minimize the total computation mse subject to a set of communication QoS constraints, and then develops an efficient AO algorithm to solve it. Section IV provides extensive simulation results to validate the effectiveness of the proposed algorithm and investigate the impact of key system parameters on performance. Finally, Section V concludes the article.

Notations: In this article, bold uppercase letters and bold lowercase letters denote matrices and column vectors, respectively. Calligraphic letters, e.g., $\mathcal{K}$, are used to denote sets. For a matrix $\mathbf{A}$, its transpose, conjugate, conjugate transpose, and inverse are denoted by $\mathbf{A}^T$, $\mathbf{A}^*$, $\mathbf{A}^H$, and $\mathbf{A}^{-1}$, respectively. For a vector $\mathbf{a}$, $||\mathbf{a}||$ represents its Euclidean (L2) norm. For a complex number z, $|z|$ and $\mathrm{Re}\{z\}$ denote its modulus and real part. $\mathbb{E}\{\cdot\}$ denotes the statistical expectation. ∇ denotes the gradient operator. $\mathrm{diag}(\mathbf{a})$ represents a diagonal matrix with the elements of vector $\mathbf{a}$ on its main diagonal. $\mathcal{CN}(\boldsymbol{\mu}, \mathbf{C})$ denotes a complex normal distribution with mean $\boldsymbol{\mu}$ and covariance matrix $\mathbf{C}$. The sets of $m \times n$-dimensional real and complex matrices are denoted by $\mathbb{R}^{m\times n}$ and $\mathbb{C}^{m\times n}$.

II. System Model

Let us consider a SIM-enhanced uplink ICC system, which consists of an N-antenna BS equipped with a uniform planar array (UPA) and K single-antenna user equipments (UEs), as illustrated in Fig. 1. Let $\mathcal{K} \triangleq \{1, \ldots, K\}$ denote the set of all UEs. The system is designed to support two concurrent tasks, namely high-reliability communication tasks and high-accuracy AirComp tasks. Based on the distinct service requirements, the set $\mathcal{K}$ is partitioned into two disjoint subsets, the communication UE set and the computation UE set, denoted by $\mathcal{K}_D$ and $\mathcal{K}_C$, respectively, such that $\mathcal{K}_D \cup \mathcal{K}_C = \mathcal{K}$ and $\mathcal{K}_D \cap \mathcal{K}_C = \emptyset$. Specifically, the communication UE set includes $K_D = |\mathcal{K}_D|$ communication UEs, with each UE $i \in \mathcal{K}_D$ transmitting an individual data symbol d_i intended for reliable decoding. The computation UE set consists of $K_C = |\mathcal{K}_C|$ computation UEs, where each UE $k \in \mathcal{K}_C$ transmits a locally preprocessed signal s_k as part of J independent AirComp tasks. For the jth Aircomp task, let $\mathcal{K}_{C,j} \subseteq \mathcal{K}_C$ denote the subset of computation UEs involved. Note that all transmitted symbols, $\{d_i\}$ and $\{s_k\}$, are assumed to be mutually independent with zero mean and unit variance.

These uplink signals are concurrently received at the BS, which is equipped with a SIM that enables advanced wavefront manipulation. In particular, SIM is assumed to feature a multi-layer architecture of L cascaded metasurfaces, each populated by M independently controllable meta-atoms, with the sets of layer and meta-atom indices denoted by $\mathcal{L} = \{1, \ldots, L\}$ and $\mathcal{M} = \{1, \ldots, M\}$, respectively. It is worth noting that although the BS employs a single set of SIM phase shifts, the massive number of meta-atoms ($L \times M$) provides sufficient DoFs to manipulate electromagnetic waves in the spatial domain. This allows the SIM to perform high-resolution spatial filtering, simultaneously creating constructive beams for AirComp UEs and nulling beams for communication UEs at their respective distinct spatial angles. By optimizing the phase shifts of these meta-atoms via a smart controller, the BS can meticulously reshape the propagation environment, thereby facilitating the harmonious coexistence of communication and computation services. Having established the system architecture, we now detail the end-to-end channel propagation and formulate the resulting received signal model.

A. Channel Model

In general, the uplink signal from the kth UE to the BS travels through three cascaded propagation paths, namely from the UE to the first layer of the SIM, across the SIM layers, and then from the last layer to the BS. First, we consider the channel between the kth UE to the SIM front surface, denoted by $\mathbf{h}_k^{\mathrm{SIM}} \in \mathbb{C}^{M\times 1}$, which is assumed to follow a Rayleigh fading distribution, i.e., $\mathbf{h}_k^{\mathrm{SIM}} \sim \mathcal{CN}(0, \beta_k \mathbf{R})$. Here, β_k represents the path loss, and the semi-positive definite matrix $\mathbf{R}$ denotes the spatial correlation among the meta-atoms on the first layer. Under the assumption of isotropic scattering with uniformly distributed multipath components, the elements of this spatial correlation matrix can be expressed as $[\mathbf{R}]_{m,m'} = \mathrm{sinc}((2D_{m,m'})/\lambda)$, where $D_{m,m'}$ is the spatial separation between the mth and m'th meta-atoms and λ is the wavelength [37].

Next, we define the transmission channel matrix from the lth layer to the $(l+1)$th layer of SIM as $\mathbf{W}_l \in \mathbb{C}^{M\times M}$, where $l \in \mathcal{L}$ and $l \leq L-1$. According to the Rayleigh–Sommerfeld diffraction theory [39], the transmission coefficient from the mth meta-atom of the lth layer to the m'th meta-atom of the $(l+1)$th layer is defined as

$$[\mathbf{W}_l]_{m',m} = \frac{A_t \cos\chi_l^{m,m'}}{D_l^{m,m'}} \left(\frac{1}{2\pi D_l^{m,m'}} - j\frac{1}{\lambda} \right) e^{j\frac{2\pi D_l^{m,m'}}{\lambda}} \tag{1}$$

where A_t is the meta-atom area, $\chi_l^{m,m'}$ is the propagation angle, and $D_l^{m,m'}$ is the propagation distance. Furthermore, for the case of $l = L$, the transmission channel matrix from the last layer of SIM to the BS antenna array as $\mathbf{W}_L \in \mathbb{C}^{N\times M}$, whose elements $[\mathbf{W}_L]_{n,m}$ can be similarly obtained by using (1).

Managed by a smart controller, each meta-atom in the SIM offers an independently tunable phase shift. To facilitate the overall system design, the complete set of $L \times M$ phase shifts is aggregated into a single vector $\boldsymbol{\theta} = [\theta_{1,1}, \ldots, \theta_{L,M}]^T \in \mathbb{R}^{LM\times 1}$, where $\theta_{l,m} \in (0, 2\pi]$ denotes the phase shift of the mth meta-atom on the lth layer. In this context, the diagonal phase control matrix for the lth layer of SIM can be represented by $\boldsymbol{\Theta}_l = \mathrm{diag}(e^{j\theta_{l,1}}, \ldots, e^{j\theta_{l,M}}) \in \mathbb{C}^{M\times M}$. Consequently, the wave-domain beamforming matrix at the BS enhanced by SIM can be expressed in the cascaded form as

$$\mathbf{G}(\boldsymbol{\theta}) = \mathbf{W}_L \boldsymbol{\Theta}_L \mathbf{W}_{L-1} \cdots \boldsymbol{\Theta}_2 \mathbf{W}_1 \boldsymbol{\Theta}_1 \in \mathbb{C}^{N\times M}. \tag{2}$$

By combining the three cascaded propagation paths, the equivalent end-to-end channel vector from the kth UE to the BS is given by

$$\mathbf{h}_k(\boldsymbol{\theta}) = \mathbf{G}(\boldsymbol{\theta}) \mathbf{h}_k^{\mathrm{SIM}} \in \mathbb{C}^{N\times 1}. \tag{3}$$

B. Signal Model

During the transmission phase, each UE sends its signal, with p_i and p_k denoting the transmit power for communication UEs and computation UEs, respectively. Then the received signal $\mathbf{y} \in \mathbb{C}^{N\times 1}$ at the BS is given by

$$\mathbf{y} = \underbrace{\sum_{i\in\mathcal{K}_D} \sqrt{p_i}\, \mathbf{h}_i(\boldsymbol{\theta})\, d_i}_{\text{Communication Signal}} + \underbrace{\sum_{k\in\mathcal{K}_C} \sqrt{p_k}\, \mathbf{h}_k(\boldsymbol{\theta})\, s_k}_{\text{Computation Signal}} + \mathbf{n} \tag{4}$$

where $\mathbf{n}$ is the additive white gaussian noise (AWGN) vector, following a complex Gaussian distribution $\mathbf{n} \sim \mathcal{CN}(0, \sigma^2 \mathbf{I}_N)$, with σ^2 representing the noise variance.

Based on the received signal $\mathbf{y}$, we now select the performance metrics for evaluating computation and communication tasks, respectively. For the jth AirComp task, the desired target function signal is denoted by $S_j^{\mathrm{target}} = \sum_{k\in\mathcal{K}_{C,j}} s_k$ by aggregating signals from a computation UE subset $\mathcal{K}_{C,j}$. To recover the desired target function, BS employs a linear computation combining vector $\mathbf{z}_{\mathrm{comp},j} \in \mathbb{C}^{N\times 1}$ to obtain an estimate of the target function, i.e., $\hat{S}_j = \mathbf{z}_{\mathrm{comp},j}^H \mathbf{y}$. In this context, the performance metric of the jth AirComp task can be measured by the mse between the S_j^{target} and $\hat{S}_j$, which is given by

$$\begin{aligned}
\mathrm{mse}_j &= \mathbb{E}\left[\left| S_j^{\mathrm{target}} - \hat{S}_j \right|^2 \right] \\
&= \sum_{k\in\mathcal{K}_{C,j}} \left| \sqrt{p_k} \mathbf{z}_{\mathrm{comp},j}^H \mathbf{h}_k(\boldsymbol{\theta}) - 1 \right|^2 \\
&\quad + \sum_{k'\in\mathcal{K}_C \setminus \mathcal{K}_{C,j}} p_{k'} \left| \mathbf{z}_{\mathrm{comp},j}^H \mathbf{h}_{k'}(\boldsymbol{\theta}) \right|^2 \\
&\quad + \sum_{i\in\mathcal{K}_D} p_i \left| \mathbf{z}_{\mathrm{comp},j}^H \mathbf{h}_i(\boldsymbol{\theta}) \right|^2 + \sigma^2 \left\| \mathbf{z}_{\mathrm{comp},j} \right\|^2.
\end{aligned} \tag{5}$$

Concurrently, for the communication tasks, the BS must reliably decode the data streams transmitted by communication UEs. To this end, it employs a dedicated communication decoding vector $\mathbf{z}_{\mathrm{data},i} \in \mathbb{C}^{N\times 1}$ for each communication UE $i \in \mathcal{K}_D$. Applying this vector to the received signal $\mathbf{y}$ yields the estimated data symbol $\hat{d}_i$ for the ith communication UE, which can be explicitly written as

$$\begin{aligned}
\hat{d}_i &= \mathbf{z}_{\mathrm{data},i}^H \mathbf{y} \\
&= \underbrace{\sqrt{p_i} \mathbf{z}_{\mathrm{data},i}^H \mathbf{h}_i(\boldsymbol{\theta})\, d_i}_{\text{Desired Signal}} + \underbrace{\sum_{i'\in\mathcal{K}_D, i'\neq i} \sqrt{p_{i'}} \mathbf{z}_{\mathrm{data},i}^H \mathbf{h}_{i'}(\boldsymbol{\theta})\, d_{i'}}_{\text{Intra-service Interference}} \\
&\quad + \underbrace{\sum_{k\in\mathcal{K}_C} \sqrt{p_k} \mathbf{z}_{\mathrm{data},i}^H \mathbf{h}_k(\boldsymbol{\theta})\, s_k}_{\text{Inter-service Interference}} + \underbrace{\mathbf{z}_{\mathrm{data},i}^H \mathbf{n}}_{\text{Noise}}
\end{aligned} \tag{6}$$

where the four terms on the right side of the equation represent the desired signal from UE i, the intraservice interference from other communication UEs in $\mathcal{K}_D$, the interservice interference from all computation UEs in $\mathcal{K}_C$, and the processed additive noise, respectively. Based on this signal decomposition, we adopt a commonly used SINR as the performance metric of communication tasks to guarantee communication QoS. Specifically, the SINR for the ith communication UE is given by (7), as shown at the bottom of the page.

III. Joint Optimization Design

As can be observed from the computation mse in (5) and communication SINR in (7), the performance of both communication and computation tasks are determined by the phase shifts of SIM $\boldsymbol{\theta}$, the transmit power p_k, the computation combining vectors $\mathbf{z}_{\text{comp},j}$, and communication decoding vectors $\mathbf{z}_{\text{data},i}$. To jointly design the SIM-enhanced ICC system, we aim to minimize the total computation mse while satisfying the communication QoS requirements, which is formulated as the following optimization problem:

$$\min_{\substack{\boldsymbol{\theta},\{p_k\}\\ \{\mathbf{z}_{\text{comp},j}\},\{\mathbf{z}_{\text{data},i}\}}} \quad \text{mse}_{\text{total}}\left(\boldsymbol{\theta},\{p_k\},\{\mathbf{z}_{\text{comp},j}\}\right) \tag{8a}$$

$$\text{s.t. } \text{SINR}_i\left(\boldsymbol{\theta},\mathbf{z}_{\text{data},i},\{p_k\}\right) \geq \Gamma_i \quad \forall i \in \mathcal{K}_D \tag{8b}$$

$$0 \leq p_k \leq P_{k,\max} \quad \forall k \in \mathcal{K} \tag{8c}$$

$$\theta_{l,m} \in [0, 2\pi) \quad \forall l \in \mathcal{L}, m \in \mathcal{M} \tag{8d}$$

where $\text{mse}_{\text{total}} = \sum_{j=1}^{J} \text{mse}_j$ is the total computation mse, Γ_i is the threshold value of SINR_i, and constraint (8c) caps each UE's transmit power at $P_{k,\max}$.

It is observed that the formulated problem (8) is a highly nonconvex optimization problem, primarily due to the intricate coupling between the receive beamforming variables and the SIM phase shifts with unit-modulus constraints. Directly seeking the global optimal solution for such high-dimensional nonconvex problems is computationally prohibitive. Conversely, traditional heuristic approaches, such as Zero-Forcing beamforming with random phase shifts or noniterative separate design schemes, optimize variables independently without iterative refinement. These methods often fail to capture the mutual dependencies, leading to unsatisfactory system performance. To strike a balance between computational tractability and optimization quality, we propose an efficient AO algorithm. This framework decomposes the intractable original problem into three tractable subproblems, i.e., BS receiver design, transmit power allocation, and SIM phase shift configuration. By solving these subproblems in an iterative manner, the AO algorithm progressively refines the solution and is guaranteed to converge to a stationary point within the feasible region, representing a high-quality suboptimal solution with polynomial complexity.

A. BS Receiver Design

First, we design the BS receiver vector $\{\mathbf{z}_{\text{comp},j}\}$ and $\{\mathbf{z}_{\text{data},i}\}$ while keeping the SIM phase shifts $\boldsymbol{\theta}$ and transmit powers $\{p_k\}$ fixed. Since the two BS receivers are independent of each other, they can be considered separately.

For the computation combining vector $\mathbf{z}_{\text{comp},j}$, the subproblem aims to minimize the mse of the jth AirComp task, which is defined as

$$\min_{\mathbf{z}_{\text{comp},j}} \quad \text{mse}_j = \mathbb{E}\left[\left|S_j^{\text{target}} - \mathbf{z}_{\text{comp},j}^H \mathbf{y}\right|^2\right]. \tag{9}$$

By expanding the squared term, the mse_j can be rewritten as the following quadratic form:

$$\begin{aligned}\text{mse}_j &= \mathbf{z}_{\text{comp},j}^H \mathbb{E}\left[\mathbf{y}\mathbf{y}^H\right]\mathbf{z}_{\text{comp},j}\\ &\quad - 2\text{Re}\left\{\mathbf{z}_{\text{comp},j}^H \mathbb{E}\left[\mathbf{y}\left(S_j^{\text{target}}\right)^*\right]\right\} + \mathbb{E}\left[\left|S_j^{\text{target}}\right|^2\right].\end{aligned} \tag{10}$$

To simplify the notation, we define the covariance matrix of the received signal as $\hat{\mathbf{Y}} = \mathbb{E}[\mathbf{y}\mathbf{y}^H]$ and the cross correlation vector as $\hat{\mathbf{y}}_j = \mathbb{E}[\mathbf{y}(S_j^{\text{target}})^*]$. The expression (10) then becomes $\text{mse}_j = \mathbf{z}_{\text{comp},j}^H \hat{\mathbf{Y}} \mathbf{z}_{\text{comp},j} - 2\text{Re}\{\mathbf{z}_{\text{comp},j}^H \hat{\mathbf{y}}_j\} + \mathbb{E}[|S_j^{\text{target}}|^2]$. Since problem (9) is an unconstrained convex quadratic programming problem, we compute the complex gradient of the mse with respect to $\mathbf{z}_{\text{comp},j}^*$ and set it to zero, i.e.,

$$\frac{\partial \text{mse}_j}{\partial \mathbf{z}_{\text{comp},j}^*} = \hat{\mathbf{Y}}\mathbf{z}_{\text{comp},j} - \hat{\mathbf{y}}_j = \mathbf{0}. \tag{11}$$

By solving this linear equation, we obtain the optimal minimum mean square error (mmse) computation combining vector in closed form as follows:

$$\mathbf{z}_{\text{comp},j}^{\text{opt}} = \hat{\mathbf{Y}}^{-1}\hat{\mathbf{y}}_j \tag{12}$$

where $\hat{\mathbf{Y}} = \sum_{k\in\mathcal{K}} p_k \mathbf{h}_k(\boldsymbol{\theta})\mathbf{h}_k^H(\boldsymbol{\theta}) + \sigma^2 \mathbf{I}_N$ and $\hat{\mathbf{y}}_j = \sum_{k\in\mathcal{K}_{C,j}} \sqrt{p_k}\,\mathbf{h}_k(\boldsymbol{\theta})$.

Next, for any given communication UE $i \in \mathcal{K}_D$, its decoding vector $\mathbf{z}_{\text{data},i}$ only appears in the SINR constraint. To provide the largest possible feasible region for the subsequent two subproblems, an effective strategy is to design the receiver to maximize its own performance metric. Therefore, we aim to find the $\mathbf{z}_{\text{data},i}$ that maximizes the SINR for UE i. This subproblem can be formulated as

$$\max_{\mathbf{z}_{\text{data},i}} \ \text{SINR}_i = \frac{p_i\left|\mathbf{z}_{\text{data},i}^H \mathbf{h}_i(\boldsymbol{\theta})\right|^2}{\sum_{k\in\mathcal{K},k\neq i} p_k \left|\mathbf{z}_{\text{data},i}^H \mathbf{h}_k(\boldsymbol{\theta})\right|^2 + \sigma^2\left\|\mathbf{z}_{\text{data},i}\right\|^2}. \tag{13}$$

To facilitate the derivation, we can express the SINR in a more compact quadratic form. Specifically, we define the desired signal's covariance matrix as $\mathbf{C}_i^{\text{des}} = p_i \mathbf{h}_i(\boldsymbol{\theta})\mathbf{h}_i^H(\boldsymbol{\theta})$ and the interference-plus-noise covariance matrix as $\mathbf{C}_i^{ipn} =$

$$\text{SINR}_i = \frac{p_i\left|\mathbf{z}_{\text{data},i}^H \mathbf{h}_i(\boldsymbol{\theta})\right|^2}{\sum_{i'\in\mathcal{K}_D,i'\neq i} p_{i'}\left|\mathbf{z}_{\text{data},i}^H \mathbf{h}_{i'}(\boldsymbol{\theta})\right|^2 + \sum_{k\in\mathcal{K}_C} p_k\left|\mathbf{z}_{\text{data},i}^H \mathbf{h}_k(\boldsymbol{\theta})\right|^2 + \sigma^2\left\|\mathbf{z}_{\text{data},i}\right\|^2} \quad \forall i \in \mathcal{K}_D \tag{7}$$

$\sum_{k\in\mathcal{K},k\neq i} p_k\mathbf{h}_k(\boldsymbol{\theta})\mathbf{h}_k^H(\boldsymbol{\theta}) + \sigma^2\mathbf{I}_N$. The problem in (13) is then equivalent to

$$\max_{\mathbf{z}_{\text{data},i}} \frac{\mathbf{z}_{\text{data},i}^H\mathbf{C}_i^{\text{des}}\mathbf{z}_{\text{data},i}}{\mathbf{z}_{\text{data},i}^H\mathbf{C}_i^{ipn}\mathbf{z}_{\text{data},i}}. \tag{14}$$

It is seen that Problem (14) is a well-known generalized Rayleigh quotient problem [40], whose solution can be obtained by finding the maximum generalized eigenvalue $\lambda_{\max}$ of the matrix pair $(\mathbf{C}_i^{\text{des}},\mathbf{C}_i^{ipn})$. The vector $\mathbf{z}_{\text{data},i}$ that achieves this maximum is the corresponding generalized eigenvector, which is the solution to the generalized eigenvalue problem $\mathbf{C}_i^{\text{des}}\mathbf{z}_{\text{data},i} = \lambda_{\max}\mathbf{C}_i^{ipn}\mathbf{z}_{\text{data},i}$. Given that $\mathbf{C}_i^{\text{des}}$ is a rank-one matrix, we can substitute its definition into the eigenvector equation

$$p_i\mathbf{h}_i(\boldsymbol{\theta})\,\mathbf{h}_i^H(\boldsymbol{\theta})\,\mathbf{z}_{\text{data},i} = \lambda_{\max}\mathbf{C}_i^{ipn}\mathbf{z}_{\text{data},i}. \tag{15}$$

Since $p_i\mathbf{h}_i^H(\boldsymbol{\theta})\mathbf{z}_{\text{data},i}$ is a scalar value, (15) reveals that the vector $\mathbf{C}_i^{ipn}\mathbf{z}_{\text{data},i}$ must be collinear with the channel vector $\mathbf{h}_i(\boldsymbol{\theta})$. Consequently, the optimal decoding vector $\mathbf{z}_{\text{data},i}$ that maximizes the SINR must be proportional to $(\mathbf{C}_i^{ipn})^{-1}\mathbf{h}_i(\boldsymbol{\theta})$, which can be expressed as

$$\mathbf{z}_{\text{data},i}^{\text{opt}} \propto \left(\mathbf{C}_i^{ipn}\right)^{-1}\mathbf{h}_i(\boldsymbol{\theta}). \tag{16}$$

It is noteworthy that this receiver structure, which maximizes the SINR, is formally identical to the well-known mmse receiver

$$\mathbf{z}_{\text{data},i}^{\text{opt}} = \left(\sum_{k\in\mathcal{K},k\neq i} p_k\mathbf{h}_k(\boldsymbol{\theta})\,\mathbf{h}_k^H(\boldsymbol{\theta}) + \sigma^2\mathbf{I}_N\right)^{-1}\mathbf{h}_i(\boldsymbol{\theta}). \tag{17}$$

Specifically, the mmse receiver's optimal strategy of first suppressing interference and then matching the desired signal's channel is precisely the linear process that maximizes the SINR. Thus, adopting the mmse structure is the ideal approach that simultaneously satisfies both critical performance criteria of minimizing estimation error and maximizing signal quality.

B. Transmit Power Allocation

Next, we consider the subproblem for transmit power allocation while the other variables kept fixed. For clarity, we first rewrite the objective function and constraints of the original problem as explicit functions of the power variables $\{p_k\}$. Based on (5), the total mse can be rewritten as

$$\text{mse}_{\text{total}} = \sum_{j=1}^{J}\left(\sum_{k\in\mathcal{K}} p_kP_{j,k}^A - 2\sum_{k\in\mathcal{K}_{C,j}}\sqrt{p_k}P_{j,k}^B + P_{j,k}^C\right) \tag{18}$$

where $P_{j,k}^A = |\mathbf{z}_{\text{comp},j}^H\mathbf{h}_k|^2$, $P_{j,k}^B = \text{Re}\{\mathbf{z}_{\text{comp},j}^H\mathbf{h}_k\}$, and $P_{j,k}^C$ are power-independent constants. Meanwhile, the SINR constraints in (8b) can be rearranged into linear inequalities (19b) with respect to power and then the subproblem can be formulated as

$$\min_{\{p_k\}} \sum_{j=1}^{J}\left(\sum_{k\in\mathcal{K}} p_kP_{j,k}^A - 2\sum_{k\in\mathcal{K}_{C,j}}\sqrt{p_k}P_{j,k}^B\right) \tag{19a}$$

$$\text{s.t.}\quad \text{(8c)}$$

$$p_i\left|\mathbf{z}_{\text{data},i}^H\mathbf{h}_i\right|^2 - \Gamma_i\sum_{k\neq i}p_k\left|\mathbf{z}_{\text{data},i}^H\mathbf{h}_k\right|^2 \geq \Gamma_i\sigma^2\left\|\mathbf{z}_{\text{data},i}\right\|^2 \quad \forall i\in\mathcal{K}_D, k\in\mathcal{K}. \tag{19b}$$

Although problem (19) is a convex optimization problem, the non-linear square root terms in its objective function render it a non-standard form, requiring reformulation before it can be solved efficiently. To address this, we employ a standard convex reformulation technique to cast the problem into an equivalent second-order cone programming (SOCP) form. Specifically, we introduce a set of auxiliary variables $\{q_k\}$, and relax the implicit equality $q_k = \sqrt{p_k}$ into the following convex inequality constraint:

$$q_k^2 \leq p_k, \quad q_k \geq 0 \quad \forall k\in\mathcal{K}. \tag{20}$$

The equivalence of this reformulation is established by the following theorem.

Theorem 1: For the optimization problem (19) with the additional constraints in (20), any optimal solution $\{p_k^*, q_k^*\}$ must satisfy the equality $(q_k^*)^2 = p_k^*$ for all $k\in\mathcal{K}$.

Proof: We prove Theorem 1 by contradiction. Assume that for the optimal solution $\{p_k^*, q_k^*\}$, there exists an index $k'\in\mathcal{K}_{C,j}$ for some task j such that $(q_{k'}^*)^2 < p_{k'}^*$. Then, let us construct a new feasible solution by setting $q_{k'}^{\text{new}} = q_{k'}^* + \epsilon$ while keeping all other variables unchanged, where $\epsilon > 0$ is a sufficiently small value such that $(q_{k'}^{\text{new}})^2 \leq p_{k'}^*$. Since the receiver is designed to align with the channel, we generally have $P_{j,k'}^B = \text{Re}\{\mathbf{z}_{\text{comp},j}^H\mathbf{h}_{k'}\} > 0$. This implies that the objective function in (19a), which contains the term $-2\sum_{k\in\mathcal{K}_{C,j}} q_kP_{j,k'}^B$, is a monotonically decreasing function with respect to $q_{k'}$. Therefore, increasing $q_{k'}^*$ to $q_{k'}^{\text{new}}$ will strictly decrease the objective value. This contradicts the initial assumption that $\{p_k^*, q_k^*\}$ is the optimal solution. Thus, the equality $(q_k^*)^2 = p_k^*$ must hold for all k at the optimal point. ■

With the above transformation, the power optimization subproblem can be finally expressed into the following standard SOCP form:

$$\min_{\{p_k\},\{q_k\}} \sum_{j=1}^{J}\left(\sum_{k\in\mathcal{K}} p_kP_{j,k}^A - 2\sum_{k\in\mathcal{K}_{C,j}} q_kP_{j,k}^B\right)$$

$$\text{s.t.}\quad \text{(8c), (19b), (20)}. \tag{21}$$

This problem is a standard convex optimization problem, as it features a linear objective function, linear inequality constraints, and second-order cone constraints. Therefore, it can be efficiently solved by convex optimization toolboxes such as CVX.

C. SIM Phase Shift Configuration

Finally, with the BS receivers and transmit powers fixed, we address the subproblem for optimizing the SIM phase shifts $\boldsymbol{\theta}$. This problem is highly non-convex due to the unit-modulus constraint on each phase shift and the intricate coupling of variables within the cascaded channel matrix. To tackle this high-dimensional challenge, we employ a block coordinate descent (BCD) framework, which decomposes the joint optimization into L more tractable, layer-wise subproblems.

Specifically, we sequentially optimize the M phase shifts of one layer at a time, while keeping the phase shifts of all other layers fixed. Now, focusing on the subproblem for the lth layer, we represent its phase shifts by the vector $\mathbf{v}_l = [v_{l,1}, \ldots, v_{l,M}]^T \in \mathbb{C}^{M\times 1}$, where $v_{l,m} = e^{j\theta_{l,m}}$. To express the end-to-end channel as an explicit function of $\mathbf{v}_l$ [28], we define the forward propagation matrix $\mathbf{F}_l$ and backward propagation matrix $\mathbf{B}_l$ as follows:

$$\mathbf{F}_l \triangleq \begin{cases} \mathbf{W}_{l-1}\boldsymbol{\Theta}_{l-1}\cdots\mathbf{W}_1\boldsymbol{\Theta}_1, & \text{if } l \neq 1 \\ \mathbf{I}_M, & \text{if } l = 1 \end{cases} \tag{22a}$$

$$\mathbf{B}_l \triangleq \begin{cases} \mathbf{W}_L\boldsymbol{\Theta}_L\cdots\mathbf{W}_{l+1}\boldsymbol{\Theta}_{l+1}\mathbf{W}_l, & \text{if } l \neq L \\ \mathbf{W}_L, & \text{if } l = L. \end{cases} \tag{22b}$$

Then, by exploiting the fact that the phase shift matrices $\{\boldsymbol{\Theta}_j\}_{j\in\mathcal{L}, j\neq l}$ are treated as constants in this BCD framework, the end-to-end channel vector can be linearly expressed as

$$\mathbf{h}_k^l = \mathbf{H}_{k,l}\mathbf{v}_l \tag{23}$$

where $\mathbf{H}_{k,l} \triangleq \mathbf{B}_l \mathrm{diag}(\mathbf{F}_l \mathbf{h}_k^{\mathrm{SIM}})$ denotes the effective channel matrix from the kth UE to the BS relative to layer l. Substituting this linear channel model, the optimization subproblem for layer l is formulated as

$$\min_{\mathbf{v}_l} \ f_{\mathrm{mse}}(\mathbf{v}_l) \tag{24a}$$
$$\text{s.t. } \mathrm{SINR}_i(\mathbf{v}_l) \geq \Gamma_i \quad \forall i \in \mathcal{K}_D \tag{24b}$$
$$|v_{l,m}| = 1 \quad \forall m \in \mathcal{M} \tag{24c}$$

where $f_{\mathrm{mse}}(\mathbf{v}_l) = \sum_{j=1}^{J} \mathrm{mse}_j(\mathbf{v}_l)$, and $\mathrm{mse}_j(\mathbf{v}_l)$ is obtained by substituting the linear channel model (23) into the original mse_j expression in (5). However, problem (24) is still difficult to solve due to the non-convex objective in (24a) and the nonconvex constraints in (24b). To this end, we adopt the successive convex approximation (SCA) strategy to approximate the nonconvex functions with simpler, convex ones at each iteration point $\mathbf{v}_l^{(t)}$.

Now, we start by addressing the nonconvex objective function $f_{\mathrm{mse}}(\mathbf{v}_l)$. Since it is a nonconvex quadratic function of $\mathbf{v}_l$, we can linearize it via a first-order Taylor expansion at the iteration point $\mathbf{v}_l^{(t)}$. Consequently, minimizing the resulting approximation is equivalent to solving

$$\min_{\mathbf{v}_l} \ \mathrm{Re}\left\{\mathbf{v}_l^H \mathbf{c}_l\right\} \tag{25}$$

where $\mathbf{c}_l \triangleq \nabla_{\mathbf{v}_l^*} f_{\mathrm{mse}}(\mathbf{v}_l^{(t)})$ is the complex gradient of the objective, which can be readily derived from (5), (23), and (24) as

$$\mathbf{c}_l = \sum_{j=1}^{J}\left(\sum_{k\in\mathcal{K}} p_k \mathbf{H}_{k,l}^H \mathbf{z}_{\mathrm{comp},j}\mathbf{z}_{\mathrm{comp},j}^H \mathbf{H}_{k,l}\mathbf{v}_l^{(t)} - \sum_{k\in\mathcal{K}_{C,j}} \sqrt{p_k}\,\mathbf{H}_{k,l}^H \mathbf{z}_{\mathrm{comp},j}\right). \tag{26}$$

Following the same approximation strategy, we handle the nonconvex SINR constraint (24b). By cross-multiplication and rearranging the terms, it can be equivalently transformed into the following nonconvex quadratic constraint:

$$g_i(\mathbf{v}_l) \triangleq \mathbf{v}_l^H \mathbf{U}_{i,l}\mathbf{v}_l - \Gamma_i \mathbf{v}_l^H \mathbf{V}_{i,l}\mathbf{v}_l - \Gamma_i\sigma^2 \left\|\mathbf{z}_{\mathrm{data},i}\right\|^2 \geq 0 \tag{27}$$

where $\mathbf{U}_{i,l} = p_i(\mathbf{H}_{i,l}^H \mathbf{z}_{\mathrm{data},i})(\mathbf{z}_{\mathrm{data},i}^H \mathbf{H}_{i,l})$ and $\mathbf{V}_{i,l} = \sum_{k\neq i, k\in\mathcal{K}} p_k(\mathbf{H}_{k,l}^H \mathbf{z}_{\mathrm{data},i})(\mathbf{z}_{\mathrm{data},i}^H \mathbf{H}_{k,l})$. Similarly, we adopt SCA technology to the nonconcave function $g_i(\mathbf{v}_l)$ at $\mathbf{v}_l^{(t)}$ and then obtain the transformed SINR constraint as

$$g_i\left(\mathbf{v}_l^{(t)}\right) + 2\mathrm{Re}\left\{\left(\mathbf{v}_l - \mathbf{v}_l^{(t)}\right)^H \mathbf{d}_{i,l}\right\} \geq 0 \tag{28}$$

where $\mathbf{d}_{i,l} \triangleq \nabla_{\mathbf{v}_l^*} g_i(\mathbf{v}_l^{(t)}) = (\mathbf{U}_{i,l} - \Gamma_i \mathbf{V}_{i,l})\mathbf{v}_l^{(t)}$ is the gradient of the function $g_i(\mathbf{v}_l)$ with respect to $\mathbf{v}_l$.

Finally, by replacing the original objective and constraints with their convex surrogates, the subproblem for SIM phase shift configuration can be rewritten as the following convex subproblem:

$$\min_{\mathbf{v}_l} \ \mathrm{Re}\left\{\mathbf{v}_l^H \mathbf{c}_l\right\} \tag{29a}$$
$$\text{s.t. } (28)$$
$$|v_{l,m}| \leq 1 \quad \forall m \in \mathcal{M}. \tag{29b}$$

We note that the relaxation to $|v_{l,m}| \leq 1$ in (29b) is not guaranteed to be tight due to the presence of the SINR constraints (28). Therefore, after obtaining the solution $\mathbf{v}_l^*$ to the relaxed subproblem (29), we employ a projection operation to map this solution back to the feasible set of the original problem (24), thus ensuring the unit-modulus constraint is strictly satisfied. Specifically, the phase shifts for the $(t+1)$th iteration are updated by normalizing the solution as follows:

$$v_{l,m}^{(t+1)} = \frac{v_{l,m}^*}{\left|v_{l,m}^*\right|} \quad \forall m \in \mathcal{M}. \tag{30}$$

After performing the projection step in (30), the BCD framework proceeds to the next layer.

Algorithm 1 Joint Design of SIM-Enhanced ICC System

Input: $N, M, L, J, K_C, K_D, \sigma^2, \{\Gamma_i\}, \{P_{k,\max}\}$.
Output: $\boldsymbol{\theta}, \{p_k\}, \{\mathbf{z}_{\mathrm{comp},j}\}, \{\mathbf{z}_{\mathrm{data},i}\}$.

```
Initialize θ^(0), {p_k^(0)}, and iteration index t = 0;
repeat
    Compute {z_comp,j^(t+1)} and {z_data,i^(t+1)} using (12) and (17) with
    θ^(t), {p_k^(t)};
    Obtain {p_k^(t+1)} by solving problem (21) via CVX;
    for l = 1 to L do
        Update v_l^(t+1) by solving the SCA subproblem (29)
        via CVX;
        Project v_l^(t+1) onto the unit modulus set using (30);
    end for
    Update t = t + 1;
until convergence
```

In summary, by alternately optimizing the three subproblems for the receiver vectors at the BS, the transmit power at the UEs and the phase shifts at the SIM, we devise an effective AO algorithm. This procedure guarantees that the objective value monotonically decreases with each iteration, ensuring the algorithm ultimately converges to a stationary point. The joint design of SIM-enhanced ICC system is formally described as Algorithm 1.

TABLE I
SIMULATION PARAMETERS

Parameters	Values
Number of BS antennas	$N = 72$
UEs	$K_C = 6, K_D = 3, J = 2$
SIM	$M = 81, L = 6$
SINR threshold	$\Gamma_i = \Gamma_0 = 3$ dB
Noise power	$\sigma^2 = -104$ dBm
Maximum transmit power	$P_{\max} = 30$ dBm

1) Complexity Analysis: The computational complexity of the proposed AO algorithm arises from the three subproblems solved within each iteration. Among them, the transmit power optimization subproblem (21) is a standard SOCP. The dimension of its optimization variables is $2K$, which is typically much smaller than the number of BS antennas N and the number of metasurface elements M. Consequently, the complexity of this step is considered negligible. Therefore, the total computational complexity per AO iteration is dominated by the BS receiver update and the SIM phase shift optimization. First, updating the mmse BS receivers involves computing the matrix inversions in (12) and (17). Since this is performed for all J computation tasks and K_D communication UEs, the complexity for this step is $\mathcal{O}((J + K_D)N^3)$. Second, the optimization of the SIM phase shifts, which represents the primary computational bottleneck, is handled via a layer-wise SCA approach. For each of the L layers, the convex subproblem (29) is solved. The complexity of solving this problem using an interior-point method is dominated by the number of optimization variables, M, resulting in a complexity of approximately $\mathcal{O}(M^{3.5})$ per SCA iteration. Denoting I_{sca} as the number of inner-loop iterations required for the SCA algorithm to converge for one layer, the total complexity for this stage is $\mathcal{O}(L \cdot I_{\text{sca}} M^{3.5})$. Combining these two dominant components, the total complexity per AO iteration can be expressed as $\mathcal{O}((J + K_D)N^3 + L \cdot I_{\text{sca}} M^{3.5})$.

Remark: The feasibility of real-time implementation relies on the relationship between the algorithm's execution time and the channel coherence time. The complexity analysis indicates that the proposed algorithm involves polynomial complexity, primarily dominated by matrix inversions and multiplications in each iteration. With modern high-performance computing hardware, e.g., FPGAs or GPUs, the execution time per coherence block can be reduced to the millisecond level. Given that SIM-based ICC systems typically operate in low-mobility scenarios, e.g., smart home or factory monitoring, with relatively long channel coherence times, the proposed joint optimization framework is feasible for practical real-time deployment.

IV. SIMULATION RESULTS

In this section, we provide a series of simulation results to verify the effectiveness of the proposed AO algorithm. Unless otherwise stated, the default simulation parameters are as shown in Table I. In our simulation, K UEs are randomly distributed within a circular area with a 300-m radius centered around the BS. The large-scale path loss is modeled as $\text{PL}_{\text{dB}} = 128.1 + 37.6 \log_{10}(d)$, where d is the distance in kilometers [38]. Additionally, the wavelength is $\lambda = c/f_0$, where the speed of light is $c = 3 \times 10^8$ m/s and the center frequency is $f_0 = 28 \times 10^9$ Hz. The thickness of the SIM is $T_{\text{SIM}} = 5\lambda$, the distance between each layer is $d_{\text{Layer}} = T_{\text{SIM}}/L$, and the size of each meta-atom is $d_x = d_y = \lambda/2$, with an area of $A_t = d_x d_y = \lambda^2/4$ [26]. All results are averaged over 100 independent random channel realizations.

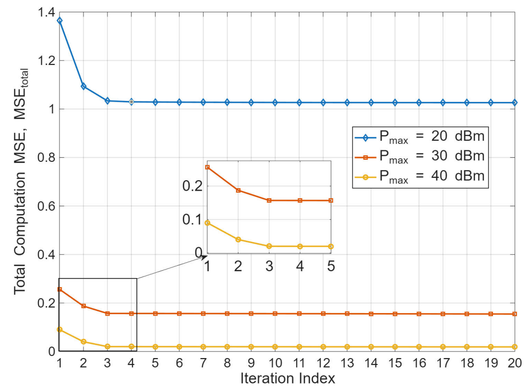

Fig. 2. Convergence behavior of the proposed Algorithm 1.

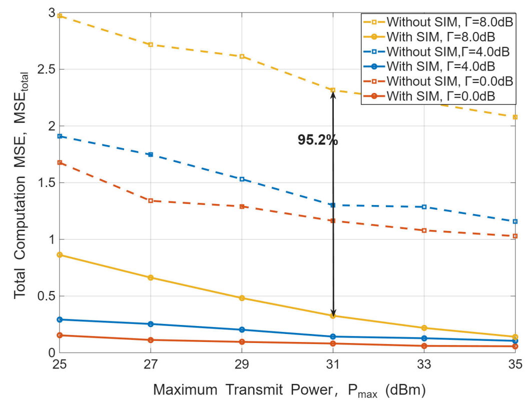

Fig. 3. Total computation mse versus maximum transmit power for schemes with and without SIM.

A. Evaluation of Computation and Communication Performance

First, we illustrate the convergence of total computation mse for Algorithm 1 under different maximum transmit powers in Fig. 2. We can observe that the total mse drops sharply within the first three iterations and reaches a stable convergence point after approximately six iterations. This indicates that the proposed AO algorithm exhibits excellent convergence performance, making it suitable for deployment in practical systems.

To verify the fundamental benefits of the proposed framework, Fig. 3 compares the performance of the SIM-enhanced scheme against a "Without SIM" benchmark, where the SIM is removed and optimization is performed only over the UE transmit powers and BS receivers. We can observe the following two general trends. First, the total computation mse for all schemes decreases as $P_{\max}$ increases. This is because a larger power budget provides the optimization algorithm with greater flexibility to suppress interference and enhance the desired signal strength for AirComp. Second, the mse increases as

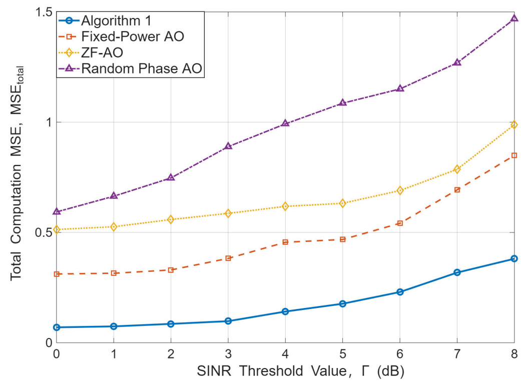

Fig. 4. Total computation mse versus SINR threshold for different schemes.

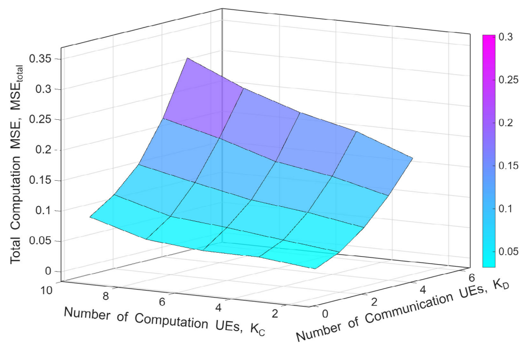

Fig. 5. Total computation mse versus the number of computation UEs and communication UEs.

the SINR threshold Γ becomes more stringent, which clearly illustrates the inherent computation-communication conflict. Against this backdrop, the fundamental advantage of our proposal is clearly validated. The SIM-enhanced scheme significantly outperforms the "Without SIM" benchmark across all tested power levels and QoS constraints. Quantitatively, the proposed SIM-enhanced scheme achieves a computation error reduction of up to 95.2% compared to the benchmark. This substantial performance gain confirms our core motivation, showing the SIM's enhanced DoF are essential for managing the inherent computation-communication conflict, particularly when facing strict communication QoS demands.

Next, Fig. 4 compares the performance of Algorithm 1 against several benchmark schemes, i.e., a Fixed-Power AO scheme by adopting $p_i = P_{\max}$, a ZF-AO scheme utilizing a Zero-Forcing receiver, and a Random Phase AO scheme with random phase shift configuration. The results clearly show that our proposed Algorithm 1 consistently achieves the lowest computation mse across all SINR thresholds, demonstrating the significant advantages of jointly optimizing all variables. Notably, the large performance gap between the proposed algorithm and the Random Phase AO scheme validates the necessity of active phase shift optimization.

Having established the algorithm's superiority, we now evaluate its performance in the core scenario of managing coexisting services. As shown in Fig. 5, we evaluate the system performance under varying service loads. It is observed that the cost of admitting different types of users is highly nonuniform. Increasing K_C results in a predictable growth in mse, primarily driven by the aggregation of noise power from more devices. Conversely, the introduction of additional

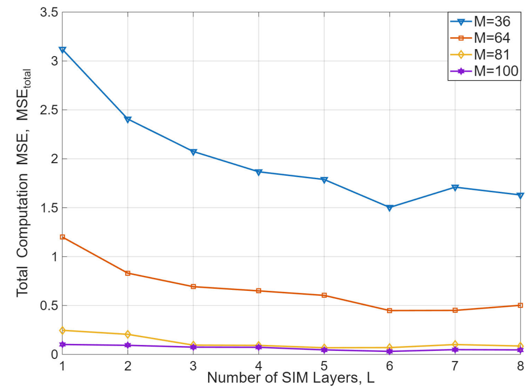

Fig. 6. Test accuracy versus communication rounds for the FL task under different schemes.

K_D imposes a severe penalty on computation performance. This phenomenon can be intuitively explained by the resource contention mechanism, where AirComp tasks share the same time-frequency resources via non-orthogonal transmission, utilizing the channel for functional computation. Communication tasks, however, impose strict SINR thresholds that act as hard constraints. Satisfying these constraints requires the SIM to prioritize interference mitigation over computation signal alignment, effectively depleting the available aperture gain and configuration flexibility. Thus, the steep slope along the K_D axis underscores that the system's capacity is effectively strictly limited by the communication load, validating the necessity of our proposed joint optimization to navigate this critical tradeoff.

To understand how system design can mitigate these performance tradeoffs, we then investigate the impact of the SIM's key architectural parameters. Fig. 6 demonstrates the impact of the number of SIM layers L and the number of elements per layer M. It can be observed that increasing the number of M can greatly enhance system performance. This is because more elements provide higher spatial resolution, allowing the algorithm to reshape the wavefront with greater precision. Notably, the performance curves exhibit a saturation point or even a slight degradation around $L = 6$, which stems from a fundamental tradeoff between wave-domain beamforming gain and severe path loss. While adding layers initially introduces more DoFs to precisely shape the wavefront, it inevitably extends the signal propagation path through the stacked structure. According to the Rayleigh–Sommerfeld diffraction theory modeled in (1), the signal suffers from multiplicative attenuation as it traverses each layer. Beyond $L = 6$, the accumulated inter-layer path loss begins to overshadow the marginal beamforming gains offered by the additional layers. Consequently, a physical ceiling is reached where increasing L no longer improves the effective SNR, indicating that simply stacking more metasurfaces does not monotonically translate to better performance.

Building on this, Fig. 7 further investigates the joint impact of the number of meta-atoms per SIM layer M and the number of BS antennas N on the total computation mse. The results reveal a clear trend that the computation mse decreases as either M or N increases. This is because a larger M provides finer-grained control over the wireless channel, enhancing the

TABLE II
HANDWRITTEN-DIGIT IDENTIFICATION RESULTS UNDER DIFFERENT SCHEMES ON IID MNIST DATASET

Data Image		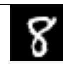				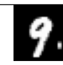		
Proposed Algorithm 1 (High Accuracy)	6	8	3	4	1	9	7	2
Without SIM (Medium Accuracy)	6	8	3	9 (×)	1	9	7	3 (×)
Random Phase (Low Accuracy)	6	2 (×)	3	9 (×)	1	0 (×)	7	8 (×)

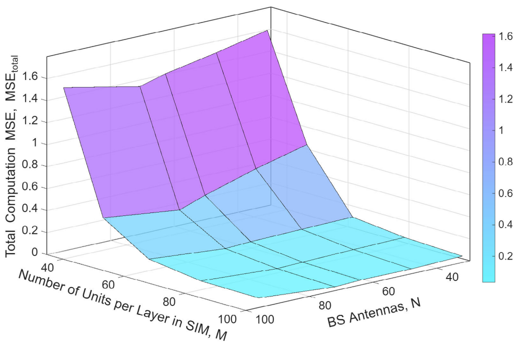

Fig. 7. Total computation mse versus the number of elements per layer and BS antennas.

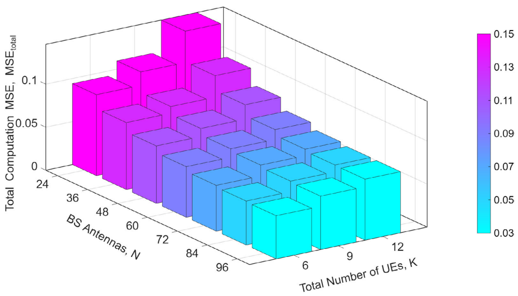

Fig. 8. Total computation mse versus the number of BS antennas and total UEs.

SIM's ability to suppress interference. Similarly, a larger N offers greater spatial multiplexing and interference nulling capabilities at the BS receiver. The combination of large-scale metasurfaces at the SIM and a massive MIMO array at the BS provides substantial DoFs, leading to a significant reduction in computation errors and showcasing a powerful synergy for future ICC systems.

Finally, Fig. 8 explores the relationship between system scale and performance, plotting the total computation mse against the number of BS antennas N and the total number of UEs K. The bar chart clearly visualizes that for a fixed number of UEs, increasing the number of antennas at the BS consistently lowers the computation mse, which is attributed to the enhanced spatial resolution for interference management. Conversely, for a fixed number of BS antennas, the mse grows as more UEs are involved in the system, highlighting the challenge of managing escalating multiuser interference. This result demonstrates a fundamental system design tradeoff that supporting a larger terminal capacity with acceptable computation accuracy requires a corresponding increase in the BS antenna array size.

B. FL Case Study

To further validate the practical efficacy of the proposed SIM-enhanced ICC framework in supporting practical applications, we conduct a case study on FL for handwritten digit recognition. Specifically, we utilize the MNIST dataset to train a convolutional neural network (CNN) in a distributed manner. The AirComp technique is employed for global model aggregation, where the computation mse minimized by our proposed algorithm directly translates to the aggregation noise added to the model updates. Crucially, this experiment is conducted under the premise of strictly guaranteeing the SINR requirements for all communication UEs. This setup allows us to verify that the proposed SIM-enhanced scheme can effectively minimize computation errors and achieve high inference accuracy while simultaneously safeguarding communication reliability, thereby validating its capability in managing the inherent conflict between heterogeneous services.

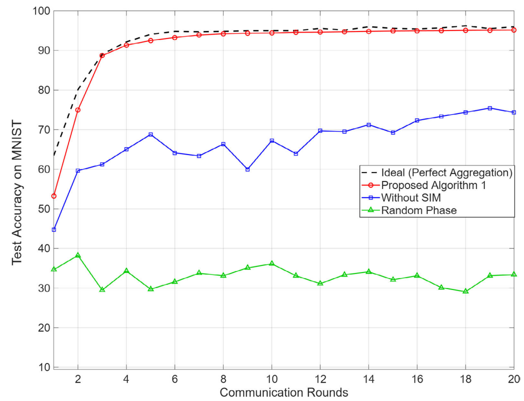

Fig. 9. Test accuracy versus communication rounds for FL task.

Fig. 9 illustrates the test accuracy versus the number of communication rounds of FL task under different schemes. It is observed that the proposed SIM-enhanced scheme achieves a learning curve that closely approximates the ideal case, rapidly converging to a high accuracy of approximately 95%. In contrast, the benchmark schemes without SIM or utilizing random phases suffer from significant aggregation noise induced by their higher computation mse, leading to slower convergence rates and unstable fluctuating accuracy. This result confirms that by proactively managing interference and reducing computation errors, the SIM-enhanced system can effectively satisfy the high-accuracy QoS requirements for ubiquitous AI applications.

Furthermore, to provide a more intuitive visualization of the impact of communication quality on FL tasks, Table II presents the identification results of specific handwritten digits under different schemes. As shown in the table, the proposed algorithm successfully recognizes all sample digits, including those with ambiguous writing styles. Conversely, other two schemes exhibit varying degrees of misclassification. For instance, the digit "2" is misclassified as "3" or "8" due to the noise corruption in the model weights. These visual examples strongly underscore that the proposed SIM-enhanced scheme effectively resolves the inherent resource conflict, achieving superior computation accuracy while strictly guaranteeing the high-quality communication.

V. Conclusion

In this article, we designed a SIM-enhanced ICC framework for uplink systems, tackling the joint optimization of BS receivers, transmit power, and SIM phase shifts via an efficient AO algorithm. The proposed algorithm not only exhibits rapid convergence, confirming its practical feasibility for dynamic environments, but also demonstrates superior performance over the benchmarks. This highlights the critical benefit of holistically optimizing the active and passive components to adeptly manage multiservice interference, thereby significantly reducing computation mse while ensuring the communication QoS. Furthermore, the results further substantiate that SIMs can effectively transform the wireless environment into a controllable, task-oriented resource, paving the way for the sophisticated ICC in future 6G wireless networks.

References

[1] C.-X. Wang et al., "On the road to 6G: Visions, requirements, key technologies, and testbeds," *IEEE Commun. Surveys Tuts.*, vol. 25, no. 2, pp. 905–974, 2nd Quart. 2023.

[2] L. Cai, Y. Dai, Q. Hu, J. Zhou, Y. Zhang, and T. Jiang, "Bayesian game-driven incentive mechanism for blockchain-enabled secure federated learning in 6G wireless networks," *IEEE Trans. Netw. Sci. Eng.*, vol. 11, no. 5, pp. 4951–4964, Sep. 2024.

[3] X. He, H. Yang, Z. Hu, and C. Lv, "Robust lane change decision making for autonomous vehicles: An observation adversarial reinforcement learning approach," *IEEE Trans. Intell. Vehicles*, vol. 8, no. 1, pp. 184–193, Jan. 2023.

[4] D. C. Nguyen et al., "6G Internet of Things: A comprehensive survey," *IEEE Internet Things J.*, vol. 9, no. 1, pp. 359–383, Jan. 2022.

[5] U. M. Malik, M. A. Javed, S. Zeadally, and S. U. Islam, "Energy-efficient fog computing for 6G-enabled massive IoT: Recent trends and future opportunities," *IEEE Internet Things J.*, vol. 9, no. 16, pp. 14572–14594, Aug. 2022.

[6] A. Şahin and R. Yang, "A survey on over-the-air computation," *IEEE Commun. Surv. Tut.*, vol. 25, no. 3, pp. 1877–1908, 3rd Quart., 2023.

[7] X. Cao, G. Zhu, J. Xu, Z. Wang, and S. Cui, "Optimized power control design for over-the-air federated edge learning," *IEEE J. Sel. Areas Commun.*, vol. 40, no. 1, pp. 342–358, Jan. 2022.

[8] Z. Wang, Y. Zhao, Y. Zhou, Y. Shi, C. Jiang, and K. B. Letaief, "Over-the-air computation for 6G: Foundations, technologies, and applications," *IEEE Internet Things J.*, vol. 11, no. 14, pp. 24634–24658, Jul. 2024.

[9] D. Fan, X. Yuan, and Y.-J.-A. Zhang, "Temporal-structure-assisted gradient aggregation for over-the-air federated edge learning," *IEEE J. Sel. Areas Commun.*, vol. 39, no. 12, pp. 3757–3771, Dec. 2021.

[10] K. Dong, S. A. Vorobyov, H. Yu, and T. Taleb, "Beamforming design for integrated sensing, over-the-air computation, and communication in Internet of Robotic Things," *IEEE Internet Things J.*, vol. 11, no. 20, pp. 32478–32489, Oct. 2024.

[11] J. Wang, Y. Li, M. Jiang, and Q. Zhang, "Orthogonal space-time block code based over-the-air computation in backscatter sensor networks," *IEEE Commun. Lett.*, vol. 28, no. 6, pp. 1442–1446, Jun. 2024.

[12] K. R. R. Ranasinghe, K. Ando, and G. T. F. de Abreu, "From theory to reality: A design framework for integrated communication and computing receivers," in *Proc. Int. Conf. Comput., Netw. Commun. (ICNC)*, Honolulu, HI, USA, Feb. 2025, pp. 865–870.

[13] Q. Qi, X. Chen, C. Zhong, and Z. Zhang, "Integrated sensing, computation and communication in B5G cellular Internet of Things," *IEEE Trans. Wireless Commun.*, vol. 20, no. 1, pp. 332–344, Jan. 2021.

[14] Q. Qi, X. Chen, A. Khalili, C. Zhong, Z. Zhang, and D. W. K. Ng, "Integrating sensing, computing, and communication in 6G wireless networks: Design and optimization," *IEEE Trans. Commun.*, vol. 70, no. 9, pp. 6212–6227, Sep. 2022.

[15] A. Tang, X. Wang, and J. A. Zhang, "Interference management for full-duplex ISAC in B5G/6G networks: Architectures, challenges, and solutions," *IEEE Commun. Mag.*, vol. 62, no. 9, pp. 20–26, Sep. 2024.

[16] K. Kim, J. Kim, and J. Joung, "A survey on system configurations of integrated sensing and communication (ISAC) systems," in *Proc. 13th Int. Conf. Inf. Commun. Technol. Converg. (ICTC)*, Oct. 2022, pp. 1176–1178.

[17] C. Huang, A. Zappone, G. C. Alexandropoulos, M. Debbah, and C. Yuen, "Reconfigurable intelligent surfaces for energy efficiency in wireless communication," *IEEE Trans. Wireless Commun.*, vol. 18, no. 8, pp. 4157–4170, Aug. 2019.

[18] Q. Wu, S. Zhang, B. Zheng, C. You, and R. Zhang, "Intelligent reflecting surface-aided wireless communications: A tutorial," *IEEE Trans. Commun.*, vol. 69, no. 5, pp. 3313–3351, May 2021.

[19] X. Gan, C. Zhong, C. Huang, and Z. Zhang, "RIS-assisted multi-user MISO communications exploiting statistical CSI," *IEEE Trans. Commun.*, vol. 69, no. 10, pp. 6781–6792, Oct. 2021.

[20] F. Guo, C. Huang, Y. Xu, Z. Yang, and M. Shikh-Bahaei, "Secure beamforming design for reconfigurable intelligent surface assisted downlink transmission," in *Proc. IEEE Int. Conf. Commun. Workshops (ICC Workshops)*, May 2022, pp. 1–6.

[21] J. V. Alegria and F. Rusek, "Channel orthogonalization with reconfigurable surfaces," in *Proc. IEEE GLOBECOM Workshops (GC Wkshps)*, Dec. 2022, pp. 37–42.

[22] D. Wen, Y. Zhou, X. Li, Y. Shi, K. Huang, and K. B. Letaief, "A survey on integrated sensing, communication, and computation," *IEEE Commun. Surv. Tut.*, vol. 27, no. 5, pp. 3058–3098, Oct. 2025.

[23] J. An, M. Debbah, T. J. Cui, Z. N. Chen, and C. Yuen, "Emerging technologies in intelligent metasurfaces: Shaping the future of wireless communications," *IEEE Trans. Antennas Propag.*, early access, May 23, 2025, doi: 10.1109/TAP.2025.3571069.

[24] Y. Zhao et al., "Multi-functional beamforming design for integrated sensing, communication, and computation," *IEEE Trans. Commun.*, vol. 73, no. 8, pp. 6322–6336, Aug. 2025.

[25] S. Tomasin, T. N. M. M. Elwakeel, A. V. Guglielmi, R. Maes, N. Noels, and M. Moeneclaey, "Analysis of challenge-response authentication with reconfigurable intelligent surfaces," *IEEE Trans. Inf. Forensics Security*, vol. 19, pp. 9494–9507, 2024.

[26] J. An et al., "Stacked intelligent metasurfaces for efficient holographic MIMO communications in 6G," *IEEE J. Sel. Areas Commun.*, vol. 41, no. 8, pp. 2380–2396, Aug. 2023.

[27] J. An, C. Yuen, L. Dai, M. Di Renzo, M. Debbah, and L. Hanzo, "Near-field communications: Research advances, potential, and challenges," *IEEE Wireless Commun.*, vol. 31, no. 3, pp. 100–107, Jun. 2024.

[28] J. An et al., "Stacked intelligent metasurface-aided MIMO transceiver design," *IEEE Wireless Commun.*, vol. 31, no. 4, pp. 123–131, Aug. 2024.

[29] J. An, Q. Wu, and R. Zhang, "Stacked intelligent metasurfaces for multi-user MISO communications," *IEEE Trans. Wireless Commun.*, vol. 22, no. 6, pp. 3848–3862, Jun. 2023.

[30] Q. Li, M. El-Hajjar, C. Xu, J. An, C. Yuen, and L. Hanzo, "Stacked intelligent metasurface-based transceiver design for near-field wide-band systems," *IEEE Trans. Commun.*, vol. 73, no. 9, pp. 8125–8139, Sep. 2025.

[31] H. Niu, X. Lei, J. An, L. Zhang, and C. Yuen, "On the efficient design of stacked intelligent metasurfaces for secure SISO transmission," *IEEE Trans. Inf. Forensics Security*, vol. 20, pp. 60–70, 2025.

[32] S. Lin, J. An, L. Gan, M. Debbah, and C. Yuen, "Stacked intelligent metasurface enabled LEO satellite communications relying on statistical CSI," *IEEE Wireless Commun. Lett.*, vol. 13, no. 5, pp. 1295–1299, May 2024.

[33] Q. Li, M. El-Hajjar, C. Xu, J. An, C. Yuen, and L. Hanzo, "Stacked intelligent metasurfaces for holographic MIMO-aided cell-free networks," *IEEE Trans. Commun.*, vol. 72, no. 11, pp. 7139–7151, Nov. 2024.

[34] G. Huang, J. An, Z. Yang, L. Gan, M. Bennis, and M. Debbah, "Stacked intelligent metasurfaces for task-oriented semantic communications," *IEEE Wireless Commun. Lett.*, vol. 14, no. 2, pp. 310–314, Feb. 2025.

[35] H. Niu, J. An, A. Papazafeiropoulos, L. Gan, S. Chatzinotas, and M. Debbah, "Stacked intelligent metasurfaces for integrated sensing and communications," *IEEE Wireless Commun. Lett.*, vol. 13, no. 10, pp. 2807–2811, Oct. 2024.

[36] Q. Zhang, Z. Du, Y. Zhao, Y. L. Guan, J. Liu, and C. Yuen, "Joint power allocation and discrete phase-shift optimization for SIM-aided ISAC systems," *IEEE Trans. Veh. Technol.*, vol. 74, no. 12, pp. 19795–19800, Dec. 2025, doi: 10.1109/TVT.2025.3584064.

[37] E. Björnson and L. Sanguinetti, “Rayleigh fading modeling and channel hardening for reconfigurable intelligent surfaces,” *IEEE Wireless Commun. Lett.*, vol. 10, no. 4, pp. 830–834, Apr. 2021.
[38] *Coordinated Multi-point Operation for LTE Physical Layer Aspects (Rel. 11)*, document TR 36.819, 3GPP, Feb. 2011.
[39] J. W. Goodman, *Introduction to Fourier Optics*, 3rd ed., Greenwood Village, CO, USA: Roberts and Company Publishers, 2005.
[40] B. D. Van Veen and K. M. Buckley, “Beamforming: A versatile approach to spatial filtering,” *IEEE ASSP Mag.*, vol. 5, no. 2, pp. 4–24, Apr. 1988.

Qiyu Chen is currently pursuing the B.S. degree with the School of Information Science and Technology, Hangzhou Normal University, Hangzhou, China.

His research interests include wireless communication, stacked intelligent metasurface, and integrated sensing, communication, and computing.

Qiao Qi (Member, IEEE) received the B.Eng. degree in electronic information engineering from Hangzhou Dianzi University, Hangzhou, China, in 2018, and the Ph.D. degree in information and communication engineering from Zhejiang University, Hangzhou, in 2023.

She is currently a Lecturer with the School of Information Science and Technology, Hangzhou Normal University, Hangzhou. Her research interests include cellular IoT, edge intelligence, and integrated sensing, communication and computing.

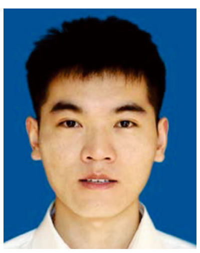

Jiancheng An (Senior Member, IEEE) received the B.S. degree in electronics and information engineering and the Ph.D. degree in information and communication engineering from the University of Electronic Science and Technology of China (UESTC), Chengdu, China, in 2016 and 2021, respectively.

From 2019 to 2020, he was a Visiting Scholar with the Next-Generation Wireless Group, University of Southampton, Southampton, U.K. From 2021 to 2023, he was a Post-Doctoral Research Fellow with the Engineering Product Development (EPD) Pillar, Singapore University of Technology and Design (SUTD), Singapore. He is currently a Research Fellow with the School of Electrical and Electronics Engineering, Nanyang Technological University (NTU), Singapore. He is the co-inventor of six patents and has published over 90 research articles in peer-reviewed international journals and conferences. His research interests include stacked intelligent metasurfaces (SIM), flexible intelligent metasurfaces (FIM), and wave-based computing.

Dr. An received the IEEE International Conference on Communications (ICC) 2023 Best Paper Award.

Zhaohui Yang (Member, IEEE) received the bachelor’s and Ph.D. degrees from Southeast University, Nanjing, China, in 2014 and 2018, respectively.

From 2018 to 2020, he was a Post-Doctoral Research Associate with the Center for Telecommunications Research, Department of Informatics, King’s College London, London, U.K. From 2020 to 2022, he was a Research Fellow with the Department of Electronic and Electrical Engineering, University College London, London. He is currently a ZJU Young Professor with Zhejiang Key Laboratory of Information Processing Communication and Networking, College of Information Science and Electronic Engineering, Zhejiang University, Hangzhou, China. His research interests include joint communication, sensing, and computation, federated learning, and semantic communication.

Dr. Yang received the IEEE Communications Society Asia-Pacific Outstanding Young Researcher Award, the IEEE Marconi Prize Paper Award, and the IEEE Katherine Johnson Young Author Paper Award. He currently serves as an Associate Editor of IEEE Transactions on Green Communications and Networking, IEEE Communications Letters, and IEEE Transactions on Machine Learning in Communications and Networking. He has served as a Guest Editor for several journals including IEEE Journal on Selected Areas in Communications.

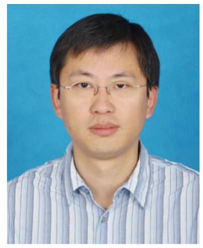

Xiaoming Chen (Senior Member, IEEE) received the B.Sc. degree in electronic engineering from Hohai University, Nanjing, China, in 2005, the M.Sc. degree in electronic engineering from Nanjing University of Science and Technology, Nanjing, in 2007, and the Ph.D. degree in electronic engineering from Zhejiang University, Hangzhou, China, in 2011.

From March 2011 to October 2016, he was with Nanjing University of Aeronautics and Astronautics, Nanjing. From February 2015 to June 2016, he was a Humboldt Research Fellow with the Institute for Digital Communications, Friedrich-Alexander-University Erlangen-Nürnberg (FAU), Erlangen, Germany. He is currently a Professor with the College of Information Science and Electronic Engineering, Zhejiang University. His research interests mainly focus on 5G/6G key techniques, Internet of Things, and smart communications.

Dr. Chen received the Best Paper Awards at the IEEE GLOBECOM in 2020, WCSP in 2020, IEEE ICC in 2019, and the IEEE/CIC ICCC in 2018. He currently serves as an Associate Editor of IEEE Transactions on Communications and IEEE Communications Letters. He has served as a Guest Editor for several journals including IEEE Journal on Selected Areas in Communications and IEEE Wireless Communications.

Chongwen Huang (Senior Member, IEEE) received the B.Sc. degree from Nankai University, Tianjin, China, in 2010, the M.Sc. degree from the University of Electronic Science and Technology of China, Chengdu, China, in 2013, and the Ph.D. degree from Singapore University of Technology and Design (SUTD), Singapore, in 2019.

From October 2019 to September 2020, he was a Post-Doctoral with SUTD. Since September 2020, he joined into Zhejiang University, Hangzhou, China, as a tenure-track young Professor. His main research interests include focused on holographic MIMO Surface/Reconfigurable intelligent surface, B5G/6G wireless communications, mmWave/THz communications, deep learning technologies for wireless communications, etc.

Dr. Huang was a recipient of the 2021 IEEE Marconi Prize Paper Award, the 2023 IEEE Fred W. Ellersick Prize Paper Award, and the 2021 IEEE ComSoc Asia-Pacific Outstanding Young Researcher Award. He has been serving as an Editor for IEEE Communications Letter, *Signal Processing* (Elsevier), *EURASIP Journal on Wireless Communications and Networking*, and *Physical Communication* since 2021.

Chau Yuen (Fellow, IEEE) received the B.Eng. and Ph.D. degrees from Nanyang Technological University (NTU), Singapore, in 2000 and 2004, respectively.

He was a Post-Doctoral Fellow with Lucent Technologies Bell Laboratories, Murray Hill, NJ, USA, in 2005, and the Institute for Infocomm Research, Singapore, from 2006 to 2010. From 2010 to 2023, he was with Singapore University of Technology and Design (SUTD), Singapore. Since 2023, he has been with the School of EEE, NTU’s. He currently serving as the Provost’s Chair in wireless communications, the Assistant Dean of the Graduate College, and the Cluster Director for Sustainable Built Environment with ERIN.

Dr. Yuen received the IEEE Communications Society Leonard G. Abraham Prize in 2024, the Best Tutorial Paper Award in 2024, the Fred W. Ellersick Prize in 2023, the IEEE Marconi Prize Paper Award in Wireless Communications in 2021, the IEEE APB Outstanding Paper Award in 2023, and the EURASIP Best Paper Award for JWCN in 2021. He is the Editor-in-Chief of *Nature Computer Science* (Springer), and an Editor of IEEE Transactions on Vehicular Technology, IEEE Transactions on Neural Networks and Learning Systems, and IEEE Transactions on Network Science and Engineering (awarded IEEE Transactions on Network Science and Engineering Excellent Editor 2024 and 2022 and a Top Associate Editor for IEEE Transactions on Vehicular Technology from 2009 to 2015). He also served as a Guest Editor for several special issues, including IEEE Journal on Selected Areas in Communications, *IEEE Wireless Communications Magazine*, *IEEE Communications Magazine*, *IEEE Vehicular Technology Magazine*, IEEE Transactions on Cognitive Communications and Networking, and *Applied Energy* (Elsevier). He has been listed as a Top 2% Scientist by Stanford University and a Highly Cited Researcher by Clarivate Web of Science since 2022.